The Astrophysical Journal, 953:181 (7pp), 2023 August 20 https://doi.org/10.3847/1538-4357/ace68a

S-type Stars: Line List for the $A^2\Pi$–$X^2\Sigma^+$ Band System of LaO

P. F. Bernath[1,2], R. Dodangodage[2], and J. Liévin[3]
[1] Department of Chemistry and Biochemistry, Old Dominion University, Norfolk, VA 23529, USA; rdodango@odu.edu
[2] Department of Physics, Old Dominion University, Norfolk, VA 23529, USA
[3] Université Libre de Bruxelles, Spectroscopy, Quantum Chemistry and Atmospheric Remote Sensing, CP 160/09, Av. F. D. Roosevelt 50, Bruxelles, Belgium
Received 2023 March 20; revised 2023 May 20; accepted 2023 July 10; published 2023 August 17

Abstract

LaO bands are found in the spectra of cool S-type stars. The bands of the $A^2\Pi$–$X^2\Sigma^+$ transition with $v' \leqslant 3$ and $v'' \leqslant 4$ are rotationally analyzed, providing spectroscopic constants for the $A^2\Pi$ state. Line strengths are calculated using an ab initio transition dipole moment function, and radiative lifetimes for the $A^2\Pi$ state have also been computed. A line list for the $A^2\Pi$–$X^2\Sigma^+$ transition of LaO is provided and can be used to determine LaO stellar abundances.

Unified Astronomy Thesaurus concepts: Spectral line lists (2082); Line intensities (2084); Spectroscopy (1558); Line positions (2085)

Supporting material: data behind figure, machine-readable tables

1. Introduction

LaO bands are prominent in S-type stars, which have approximately equal carbon and oxygen abundances. La is formed in the *s*-process by repeated neutron absorption followed by β-decay and in the *r*-process in the merger of neutron stars (Johnson 2019). La^+ atomic lines are typically used to determine La abundances, but for cooler objects, LaO is used (MacConnell et al. 2000). Two LaO band heads at λ7403 and λ7910, corresponding to the 0–0 vibrational band of the $A^2\Pi_{3/2}$–$X^2\Sigma^+$ and $A^2\Pi_{1/2}$–$X^2\Sigma^+$ subbands from the two spin–orbit components in the A state (respectively), are strong characteristic absorption features in S-type stars in near-infrared spectra (Keenan 1948; Nassau 1956).

Over the years, the spectra of LaO have been studied many times starting with a vibrational analysis of many electronic transitions by Jevons (1928). There was some confusion over the identity of the ground state, but Weltner et al. (1967) proved that LaO had an $X^2\Sigma^+$ ground state with a large magnetic hyperfine structure (^{139}La has a nuclear spin (I) of 7/2 and a magnetic moment (μ_B) of 2.78 Bohr magnetons (Steimle & Virgo 2002)). Bernard & Sibaï (1980) carried out a global fit of all data available at that time and provided a set of spectroscopic constants for the $X^2\Sigma^+$, $A'^2\Delta$, $A^2\Pi$, $B^2\Sigma^+$, and $C^2\Pi$ states. Bernard & Vergès (2000) recorded infrared spectra of the $A^2\Pi$–$A'^2\Delta$ band system and derived a set of equilibrium constants. Dipole moments for the $A^2\Pi$ and $B^2\Sigma^+$ states and hyperfine parameters for the $A^2\Pi$ were determined by Steimle & Virgo (2002). The ground $X^2\Sigma^+$ state is well characterized by microwave (Törring et al. 1988; Suenram et al. 1990) and radio frequency spectroscopy (Childs et al. 1986). More recently, the LaO ionization potential of 5.2446 eV has been measured by Cao et al. (2021), and the $B^2\Sigma^+$–$X^2\Sigma^+$ system has been reanalyzed (Bernath et al. 2022), including a line list calculation.

We report a reanalysis of the $A^2\Pi$–$X^2\Sigma^+$ system up to $v = 3$ in the excited state. Line strengths have been calculated using an ab initio transition dipole moment (TDM) function and this work provides a line list for the $A^2\Pi$–$X^2\Sigma^+$ transition.

2. Experiment

The experimental observations were as described in our $B^2\Sigma^+$–$X^2\Sigma^+$ analysis (Bernath et al. 2022). In brief, the LaO spectrum was recorded in emission from a carbon tube furnace with the Fourier transform spectrometer associated with the McMath–Pierce Solar Telescope on Kitt Peak in Arizona. The sample had a nominal temperature of 2100 °C and the spectrum covered the 350–1100 nm range.

Figure 1 is an overview of the $\Delta v = 0$ vibrational sequence of the $A^2\Pi$–$X^2\Sigma^+$ transition of LaO. The large spin–orbit coupling splits the $A^2\Pi$ state into $A^2\Pi_{3/2}$ and $A^2\Pi_{1/2}$ spin components separated by about 860 cm^{-1}. The $A^2\Pi_{3/2}$–$X^2\Sigma^+$ subband lies at higher wavenumbers (lower wavelength) than the $A^2\Pi_{1/2}$–$X^2\Sigma^+$ subband (Figure 1).

3. Ab Initio Calculations

Internally contracted multireference configuration interaction calculations (ic-MRCI; Knowles & Werner 1988; Werner & Knowles 1988) have been performed with the MOLPRO quantum chemistry package (Werner et al. 2012, 2019) to calculate the electric TDM curve for the $A^2\Pi$–$X^2\Sigma^+$ transition. A detailed description of the method, basis sets, and active space is given in our previous work on the $B^2\Sigma^+$–$X^2\Sigma^+$ transition (Bernath et al. 2022). The transition matrix elements of the electric dipole moment operator were obtained using the wave functions calculated as in Bernath et al. (2022) for the $X^2\Sigma^+$ state and through a state-averaged complete active space self-consistent field (SA-CASSCF) orbital optimization involving the two low-lying $^2\Pi$ interacting states for the $A^2\Pi$ state. A biorthogonal orbital transformation has been applied for this calculation.

TDMs were calculated at a set of internuclear distances (R), ranging from 1.6 to 2.5 Å, in steps of 0.05 Å and interpolated by B-splines to create a set of 1592 points. This ab initio TDM

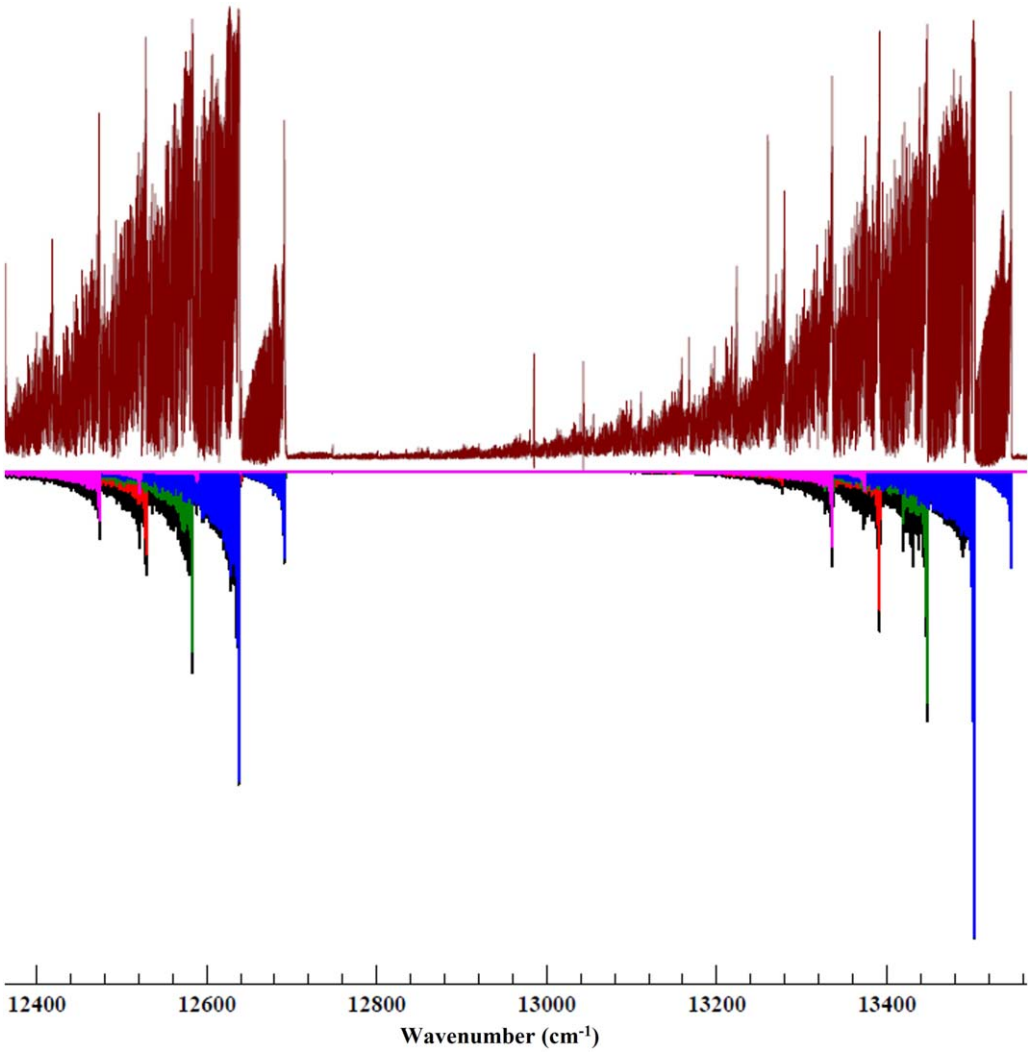

Figure 1. Overview emission spectrum of LaO (above) and simulation (below) of the $\Delta v = 0$ sequence of the $A^2\Pi$–$X^2\Sigma^+$ transition. $A^2\Pi_{3/2}$–$X^2\Sigma^+$ is on the right and $A^2\Pi_{1/2}$–$X^2\Sigma^+$ is on the left (blue: 0–0 band, green: 1–1 band, red: 2–2 band, and pink: 3–3 band).

curve is shown in Figure 2; calculated points and the interpolated values are provided as supplementary data.

4. Rotational Analysis, Spectroscopic Parameters, and Line Positions

The structure of the $X^2\Sigma^+$ state is well known from the work of Childs et al. (1986), Törring et al. (1988), Steimle & Virgo (2002), and Bernath et al. (2022). The rotational energy levels of the ground $X^2\Sigma^+$ state display $b_{\beta s}$ coupling because the Fermi contact parameter (b) that describes the hyperfine interaction is much larger than the spin–rotation interaction parameter, γ (Bacis et al. 1973; Steimle & Virgo 2002; Brown & Carrington 2003; Bernath et al. 2022). The spectroscopic parameters for the ground state ($X^2\Sigma^+$) are described in Bernath et al. (2022) and these values are used in this analysis for the $X^2\Sigma^+$ state.

The rotational structure of the $A^2\Pi$ state is fitted using the standard N^2 Hamiltonian ($H_{\rm rot}$), where $\boldsymbol{N}$ is the rotational angular momentum ($\boldsymbol{N} = \boldsymbol{J} - \boldsymbol{S}$), $\boldsymbol{J}$ is the total angular momentum excluding nuclear spin, $\boldsymbol{S}$ is the total electron spin, B is the rotational constant, and D and H are centrifugal distortion constants (Brown & Carrington 2003):

$$H_{\rm rot} = B\boldsymbol{N}^2 - D\boldsymbol{N}^4 + H\boldsymbol{N}^6. \quad (1)$$

Both electron spin and orbital angular momentum of the $A^2\Pi$ state influence the rotational structure, and the spin–orbit coupling is introduced as $H_{\rm so}$ (Hirota et al. 1994):

$$H_{\rm so} = AL_zS_z + \frac{A_D}{2}[\boldsymbol{N}^2, L_zS_z]_+ + \frac{A_H}{2}[\boldsymbol{N}^4, L_zS_z]_+, \quad (2)$$

$$[O, Q]_+ = OQ + QO, \quad (3)$$

in which A is the spin–orbit coupling constant, A_D and A_H are centrifugal distortion constants of A, $\boldsymbol{L}$ is the orbital angular momentum, and $\boldsymbol{S}$ is the electron spin angular momentum. $^2\Pi$ states also exhibit Λ type doubling, which is described by the parameters p and q (Brown & Merer 1979):

$$H_{\rm ld} = -\tfrac{1}{2}p(e^{-2i\phi}N_+S_+ + e^{2i\phi}N_-S_-) + \tfrac{1}{2}q(e^{-2i\phi}N_+^2 + e^{2i\phi}N_-^2). \quad (4)$$

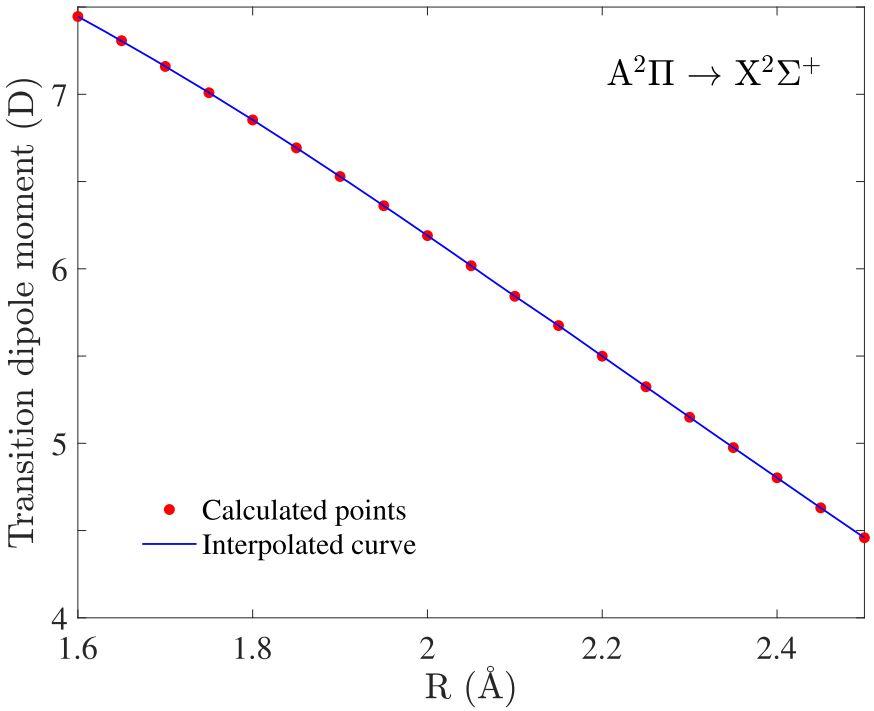

Figure 2. Ab initio transition dipole moment curve for the $A^2\Pi$–$X^2\Sigma^+$ transition of LaO.
(The data used to create this figure are available.)

Table 1
Spectroscopic Constants for the $A^2\Pi$ State

	$v = 0$	$v = 0$[a]	$v = 1$	$v = 1$[a]	$v = 2$	$v = 3$
T_v	13066.6492(11)	13066.951(11)	13824.2952(48)	13824.166(10)	14577.6096(18)	15326.4404(50)
B_v	0.34633907(84)	0.346162(82)	0.3447145(55)	0.344564(63)	0.3431243(12)	0.3414104(39)
$10^7 D_v$	2.8714(15)	2.741(78)	3.2744(224)	2.891(80)	2.8755(20)	2.7838(67)
$10^{12} H_v$	…	…	6.230(313)	…	…	…
A_v	862.4104(20)	862.434(22)	861.5701(96)	862.434	860.5999(36)	860.0181(60)
$10^4 A_{Dv}$	1.9537(83)	3.095(97)	0.90(12)	3.1	2.422(26)	0.190(20)
$10^8 A_{Hv}$	…	-0.77(12)	−6.643(450)	…	…0.276(41)	…
$10^{-12} A_{Lv}$	…	…	9.698(630)	…	…	…
p_v	−0.237942(95)	−0.26743(24)	−0.21823(38)	−0.267	−0.242335(80)	−0.22721(14)
$10^5 p_{Dv}$	0.0631(30)	…	−1.3443(240)	…	−0.0163(19)	0.1421(47)
$10^9 p_{Hv}$	…	…	1.131(30)	…	…	…
$10^2 q_v$	−0.0275(36)	−0.0096(100)	−1.030(12)	−0.0096	…	…
$10^7 q_{Dv}$	0.298(49)	…	8.94(28)	…	…	…
$10^3 a$	7.74[b]	…	7.74[b]	…	7.74[b]	7.74[b]
$10^3 c$	−8.71[b]	…	−8.71[b]	…	−8.71[b]	−8.71[b]
$10^2 d$	1.37[b]	…	1.37[b]	…	1.37[b]	1.37[b]

Notes. One standard deviation is given in parentheses (all values are in cm^{-1}).
[a] Values reported by Bernard & Sibaï (1980). Note that a slightly different Hamiltonian was used.
[b] Held fixed during fitting. Values are from Steimle & Virgo (2002).

The hyperfine interaction is described by the Frosh and Foley parameters a, b, c, and d (Steimle & Virgo 2002):

$$H_{\rm hfs} = aL_zS_z + b\boldsymbol{I}\cdot\boldsymbol{S} + c\left[I_zS_z - \tfrac{1}{3}\boldsymbol{I}\cdot\boldsymbol{S}\right] + \tfrac{d}{2}[e^{2i\phi}I_-S_- + e^{-2i\phi}I_+S_+]. \quad (5)$$

Due to the zero spin density of the unpaired electron at the La nucleus, Steimle & Virgo (2002) constrained the Fermi contact parameter (b) to zero for the $A^2\Pi$ state. The effective Hamiltonian ($H_{\rm eff}$) for LaO $A^2\Pi$ states is thus

$$H_{\rm eff} = H_{\rm rot} + H_{\rm so} + H_{\rm ld} + H_{\rm hfs}. \quad (6)$$

The rotational analysis of the LaO $A^2\Pi$–$X^2\Sigma^+$ transition was carried out with this Hamiltonian with Hund's case (a) basis functions using the PGOPHER program (Western 2017).

Table 2
Sample of Observed and Calculated Line List of the A–X Transition

F'	p'	F''	p''	Obs (cm^{-1})	Calc (cm^{-1})	Obs-Calc (cm^{-1})	Line Assignment
43	f	43	e	13502.8655	13502.8517	0.0138	rQ21(39.5)43,43 : A2Pi $v = 0$ 39.5 40 F2f 43–X2Sigma+ $v = 0$ 39.5 39 F1e 43
42	e	42	f	13502.8655	13502.8607	0.0048	rQ21(39.5)42,42 : A2Pi $v = 0$ 39.5 40 F2f 42–X2Sigma+ $v = 0$ 39.5 39 F1e 42
41	f	41	e	13502.8655	13502.8701	−0.0046	rQ21(39.5)41,41 : A2Pi $v = 0$ 39.5 40 F2f 41–X2Sigma+ $v = 0$ 39.5 39 F1e 41
40	e	40	f	13502.8655	13502.88	−0.0145	rQ21(39.5)40,40 : A2Pi $v = 0$ 39.5 40 F2f 40–X2Sigma+ $v = 0$ 39.5 39 F1e 40
44	f	44	e	13502.7856	13502.769	0.0166	rQ21(40.5)44,44 : A2Pi $v = 0$ 40.5 41 F2f 44–X2Sigma+ $v = 0$ 40.5 40 F1e 44
43	e	43	f	13502.7856	13502.7783	0.0073	rQ21(40.5)43,43 : A2Pi $v = 0$ 40.5 41 F2f 43–X2Sigma+ $v = 0$ 40.5 40 F1e 43
42	f	42	e	13502.7856	13502.7879	−0.0023	rQ21(40.5)42,42 : A2Pi $v = 0$ 40.5 41 F2f 42–X2Sigma+ $v = 0$ 40.5 40 F1e 42
41	e	41	f	13502.7856	13502.798	−0.0124	rQ21(40.5)41,41 : A2Pi $v = 0$ 40.5 41 F2f 41–X2Sigma+ $v = 0$ 40.5 40 F1e 41
40	f	40	e	13502.7856	13502.8085	−0.0229	rQ21(40.5)40,40 : A2Pi $v = 0$ 40.5 41 F2f 40–X2Sigma+ $v = 0$ 40.5 40 F1e 40
45	f	45	e	13502.7091	13502.6753	0.0338	rQ21(41.5)45,45 : A2Pi $v = 0$ 41.5 42 F2f 45–X2Sigma+ $v = 0$ 41.5 41 F1e 45
44	e	44	f	13502.7091	13502.6847	0.0244	rQ21(41.5)44,44 : A2Pi $v = 0$ 41.5 42 F2f 44–X2Sigma+ $v = 0$ 41.5 41 F1e 44
43	f	43	e	13502.7091	13502.6946	0.0145	rQ21(41.5)43,43 : A2Pi $v = 0$ 41.5 42 F2f 43–X2Sigma+ $v = 0$ 41.5 41 F1e 43
42	e	42	f	13502.7091	13502.7049	0.0042	rQ21(41.5)42,42 : A2Pi $v = 0$ 41.5 42 F2f 42–X2Sigma+ $v = 0$ 41.5 41 F1e 42

Note. F' and F'' are the total angular momentum of the A and X states, respectively. p is the parity. Obs is the observed line position in cm^{-1}; Calc is the calculated line position in cm^{-1}; Obs-Calc is the difference of the observed and calculated line positions in cm^{-1}. Line assignment illustrate the transition ${}^{\Delta N}\Delta J_{(F'^{i})F''_{j}}(J'')F'$, F'' : $A^2\Pi$ v J' N' $F1p/F2p$ F'–$X^2\Sigma^+$ v J'' N'' $F1p/F2p$ F''.

(This table is available in its entirety in machine-readable form.)

Table 3
Equilibrium Constants of LaO for $X^2\Sigma^+$ and $A^2\Pi$ States[a]

	$X^2\Sigma^+$	$A^2\Pi$
ω_e	816.9969[b]	762.104(37)
$\omega_e x_e$	2.1243[b]	2.209(11)
$10^3\omega_e y_e$	−3.48[b]	…
B_e	0.352520046[c]	0.347149(18)
$10^3\alpha_e$	1.42365[c]	1.615(12)
$10^6\gamma_e$	−2.9724[c]	…

Notes.
[a] All values are in cm^{-1}.
[b] Held fixed during fitting. Values are from Bernath et al. (2022).
[c] Held fixed during fitting. Values from Dunham constants of Törring et al. (1988).

The rotational spectroscopic parameters, hyperfine parameters, and the vibrational origins for the $X^2\Sigma^+$ state are from our previous analysis of the $B^2\Sigma^+$–$X^2\Sigma^+$ transition (Bernath et al. 2022). The equilibrium constants from Bernard & Vergès (2000) were used to calculate starting values for the origins, B, D, A, and p in the vibrational levels $v = 0$ to 3 of the excited $A^2\Pi$ state. The fitted values for nuclear hyperfine structure by Steimle & Virgo (2002) were used in our analysis for all vibrational levels of the A state and were held fixed during the fitting. The final fitted spectroscopic constants, including the band origins for the $A^2\Pi$ state, are given in Table 1.

In the analysis, 8068 lines were assigned in the 0–0, 1–1, 2–2, 3–3, 3–4, 2–3, 1–2, 0–1, 1–0, 2–1, and 3–2 bands. Maximum J'' values are 75.5, 90.5, 79.5, 40.5, 75.5, 78.5, 80.5, 82.5, 44.5, 85.5, and 72.5 for the 0–0, 1–1, 2–2, 3–3, 3–4, 2–3, 1–2, 0–1, 1–0, 2–1, and 3–2 bands, respectively. A sample of the observed and calculated line positions are given in Table 2. The labeling for the lines provided is ${}^{\Delta N}\Delta J_{(F'^{i})(F''_{j})}(J'')F'$, F'', in which N is the quantum number for total angular momentum without electron spin, subscripted $F_{i,j}$ are the customary labels for the two spin components of a $^2\Pi$ and a $^2\Sigma^+$ state, 1 has $J = N + 1/2$ and 2 has $J = N - 1/2$ (for the A state, 1 is $^2\Pi_{1/2}$ and 2 is $^2\Pi_{3/2}$), and the trailing F' and F'' are the total angular momentum with nuclear spin. Primes represent the upper A state and the double primes are for the lower X state.

5. Line Strengths and Line Lists

Line strength calculations are based on ab initio TDM calculations and RKR (Rydberg-Klein-Rees) potential curves. Le Roy's RKRprogram (Le Roy 2017a) was used to calculate the RKR potential curves. The equilibrium constants for the $X^2\Sigma^+$ were taken from Bernath et al. (2022), and for the excited $A^2\Pi$ state, rotational constants and band origins from Table 1 were fitted with the equations:

$$G_v = \omega_e\left(v + \frac{1}{2}\right) - \omega_e x_e\left(v + \frac{1}{2}\right)^2 + \omega_e y_e\left(v + \frac{1}{2}\right)^3 \quad (7)$$

$$B_v = B_e - \alpha_e\left(v + \frac{1}{2}\right) + \gamma_e\left(v + \frac{1}{2}\right)^2. \quad (8)$$

The calculated equilibrium constants are shown in Table 3 and were used as inputs to the RKR program. The two RKR potentials and TDM points were input to Le Roy's LEVEL program (Le Roy 2017b) to calculate transition dipole matrix elements $<\psi_{e'v'}|\mu|\psi_{e''v''}>$. The matrix elements were calculated for the levels connecting $v'' = 0 - 4$ and $v' = 0 - 3$, and are given in Table 4. These values were used as band strengths for the simulated bands in PGOPHER. The $A^2\Pi$–$X^2\Sigma^+$ line list was generated for $J'' < 200$ (Table 5).

The Einstein $A_{v'\rightarrow v''}(s^{-1})$ values for each band were calculated using $A_{v'\rightarrow v''} = 3.136 \times 10^{-7}\nu^3\mu^2_{v'\rightarrow v''}$ (Bernath 2020), where ν is the band origin for A–X $v' - v''$ transition in cm^{-1} and $\mu_{v'\rightarrow v''}$ is the transition moment (debye) given in Table 4. The lifetime (τ) for each vibrational level of the $A^2\Pi$ state was calculated using all radiative rates connecting the upper vibrational level (v') to all lower vibrational levels

Table 4
Band Strengths from LEVEL

	v''				
v'	0	1	2	3	4
0	6.62051	1.10032	0.201760	2.56126×10^{-2}	3.15113×10^{-3}
1	−1.36251	6.35614	1.55011	0.352263	5.19018×10^{-2}
2	0.140159	−1.93922	6.07417	1.88565	0.499735
3	5.10630×10^{-3}	0.262560	−2.38161	5.77639	2.15735

Note. All values are in debye.

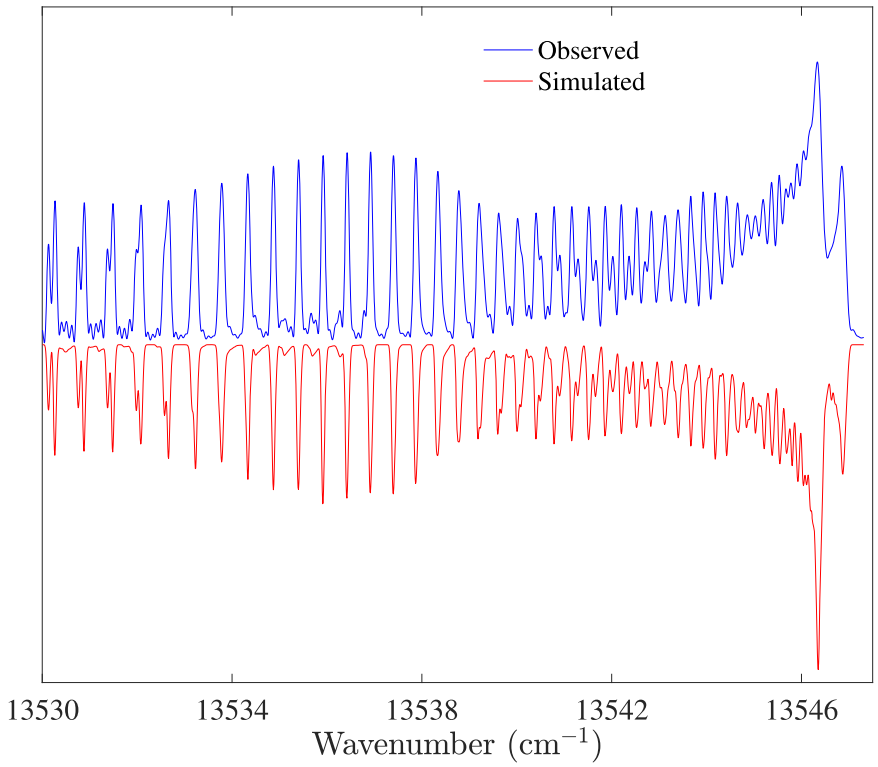

Figure 3. The 0–0 band of the $A^2\Pi_{3/2}$–$X^2\Sigma^+$ transition. (The observed spectrum is above and the simulated is below).

(v''):

$$\tau_{v'} = \frac{1}{\sum_{v''=0}^{4} A_{v' \to v''}}. \quad (9)$$

The calculated radiative lifetimes for the vibrational levels of the $A^2\Pi$ state are given in Table 6.

6. Discussion

The $A^2\Pi$–$X^2\Sigma^+$ transition of LaO has a very dense spectrum (Figure 1). A closer look at the 0–0 band of the $A^2\Pi_{3/2}$–$X^2\Sigma^+$ subband is given in Figure 3. Although the simulated 0–0 band matches the experimental spectrum, other band heads calculated from this analysis differ slightly from the observed band heads. The averaged residual error (observed-calculated) for the observed and calculated line positions is 0.0267 cm^{-1}. Overall, the simulated spectrum matches with the observed $A^2\Pi$–$X^2\Sigma^+$ transition of LaO.

Many of the spectroscopic constants for the $A^2\Pi$ state in Table 1 are irregular functions of v. The constants for $v = 1$, in particular, deviate from the expected pattern, and many nonphysical spectroscopic constants were included in the fit. The excited vibrational levels of the A state are globally perturbed. The equilibrium vibrational frequency of 762 cm^{-1} is relatively close to the spin–orbit constant of 862 cm^{-1} causing an internal perturbation in the $A^2\Pi$ state (i.e., $v = 0$ $^2\Pi_{3/2}$ with $v = 1$ $^2\Pi_{1/2}$, $v = 1$ $^2\Pi_{3/2}$ with $v = 2$ $^2\Pi_{1/2}$, $v = 2$ $^2\Pi_{3/2}$ with $v = 3$ $^2\Pi_{1/2}$, etc.). This interaction was noted previously by Bernard & Vergès (2000). We also tried including this interaction explicitly but the fits were not satisfactory, so, in the end, we decided to use a large number of empirical constants to describe the energy levels.

The spectroscopic constants for the ground state were taken from the reanalysis of the $B^2\Sigma^+$–$X^2\Sigma^+$ transition (Bernath et al. 2022) and the constants for the $A^2\Pi$ state up to $v = 3$ were determined. Bernard & Sibaï (1980) reported the origins of $v = 0$ and 1 of the $A^2\Pi$ state to be 13066.951(11) cm^{-1} and 13824.166(10) cm^{-1}, respectively. Our calculated values for the same vibrational levels (Table 1) are the same within error. The $A^2\Pi$ state lies about 5000 cm^{-1} below the $B^2\Sigma^+$ state. The unpaired electron in the $B^2\Sigma^+$ and $A^2\Pi$ states can be approximated as atomic 5p electrons. In this pure precession

Table 5
Sample Line List for the A–X Transition

F'	F''	Position (cm^{-1})	E_{up} (cm^{-1})	E_{low} (cm^{-1})	A (s^{-1})	Line Assignment
200	200	11320.5092	26810.0446	15489.5355	314729.9	pP1(202.5)200,200 : A2Pi $v = 1$ 201.5 201 F1e 200–X2Sigma+ $v = 2$ 202.5 202 F1e 200
199	200	11320.5154	26810.0509	15489.5355	85673.51	pP1(202.5)199,200 : A2Pi $v = 1$ 201.5 201 F1e 199–X2Sigma+ $v = 2$ 202.5 202 F1e 200
199	199	11320.5719	26810.0509	15489.479	435574.2	pQ12(201.5)199,199 : A2Pi $v = 1$ 201.5 201 F1e 199–X2Sigma+ $v = 2$ 201.5 202 F2f 199
198	199	11320.5781	26810.0572	15489.479	65665.48	pQ12(201.5)198,199 : A2Pi $v = 1$ 201.5 201 F1e 198–X2Sigma+ $v = 2$ 201.5 202 F2f 199
198	198	11320.6716	26810.0572	15489.3855	830192.2	pQ12(201.5)198,198 : A2Pi $v = 1$ 201.5 201 F1e 198–X2Sigma+ $v = 2$ 201.5 202 F2f 198
199	199	11320.8984	26810.0509	15489.1525	394513	pP1(202.5)199,199 : A2Pi $v = 1$ 201.5 201 F1e 199–X2Sigma+ $v = 2$ 202.5 202 F1e 199
198	199	11320.9046	26810.0572	15489.1525	66766.19	pP1(202.5)198,199 : A2Pi $v = 1$ 201.5 201 F1e 198–X2Sigma+ $v = 2$ 202.5 202 F1e 199
200	200	11320.9491	26810.0446	15489.0956	515292.9	pQ12(201.5)200,200 : A2Pi $v = 1$ 201.5 201 F1e 200–X2Sigma+ $v = 2$ 201.5 202 F2f 200
199	200	11320.9554	26810.0509	15489.0956	46800.07	pQ12(201.5)199,200 : A2Pi $v = 1$ 201.5 201 F1e 199–X2Sigma+ $v = 2$ 201.5 202 F2f 200

Notes. F' and F'' are the total angular momentum of the A and X states, respectively. Position is the line position in cm^{-1}. E_{up} and E_{low} are the energies of the A and X states in cm^{-1}. Einstein A coefficients in s^{-1} are given under A. Line assignment illustrates the transition ${}^{\Delta N}\Delta J_{(F'^{i_j})F_j''}(J'')F'$, F'' : $A^2\Pi$ v J' N' $F1p/F2p$ F'–$X^2\Sigma^+$ v J'' N'' $F1p/F2p$ F''.

(This table is available in its entirety in machine-readable form.)

Table 6
Radiative Lifetimes of LaO in the $A^2\Pi$ State

$A^2\Pi$ $v=$	0	1	2	3
τ_n (ns)	31.86	32.39	32.92	33.67

approximation (Lefebvre-Brion & Field 2004), the spin–rotation constant (γ) of the $B^2\Sigma^+$ state and the Λ-doubling constant (p) of the $A^2\Pi$ state are given by

$$p = \frac{2ABl(l+1)}{\Delta E} = \frac{4AB}{\Delta E} \approx \gamma, \quad (10)$$

in which ΔE is the energy difference between the $A^2\Pi$ and $B^2\Sigma^+$ states. For $v=0$ of the $A^2\Pi$ state, p is calculated to be -0.250 cm^{-1} compared to the observed value of -0.238 cm^{-1}, and γ for $v=0$ of the $B^2\Sigma^+$ state is -0.254 cm^{-1}. Schoonveld & Sundaram (1974) have determined equilibrium constants separately for each spin component of the A state, for $A^2\Pi_{1/2}$ $\omega_e = 762.57$ cm^{-1}, and $\omega_e x_e = 2.224$ cm^{-1}, and for $A^2\Pi_{3/2}$ $\omega_e = 761.60$ cm^{-1}, and $\omega_e x_e = 2.235$ cm^{-1}. Bernard & Sibaï (1980), in their analysis, provided the average $\omega_e = 762.09$ cm^{-1}, $\omega_e x_e = 2.230$ cm^{-1} from Schoonveld & Sundaram (1974), and deduced $B_e = 0.34696$ cm^{-1}, and $\alpha_e = 1.60 \times 10^{-3}$ cm^{-1}. Bernard & Vergès (2000) present $\omega_e = 762.0746$ cm^{-1}, $\omega_e x_e = 2.18484$ cm^{-1}, and $\omega_e y_e = -0.189 \times 10^{-2}$ cm^{-1} along with $B_e = 0.3471671(36)$ cm^{-1}, $\alpha_e = 1.6094(14) \times 10^{-3}$ cm^{-1}, and $\gamma_e = 2.531(81) \times 10^{-6}$ cm^{-1} for the $A^2\Pi$ state. In our analysis of the A–X transition, vibrational levels from $v'=0$ up to $v'=3$ were obtained, and for calculating equilibrium constants a two-parameter fit was implemented. Our calculated values (Table 3) are in good agreement with the values reported in the literature.

Radiative lifetimes for $B^2\Sigma^+$, $C^2\Pi_{1/2}$, and $C^2\Pi_{3/2}$ have been experimentally measured (Liu & Parson 1977; Carette & Bencheikh 1994), but there are no measurements of lifetimes for the $A^2\Pi$ state. Ying & Gang (2020) have calculated radiative lifetimes of the $A^2\Pi$ state for $v=0$ to 5 with values ranging from 34.18 to 36.74 ns. Our computed radiative lifetimes (Table 6) are similar.

7. Conclusion

Spectroscopic constants up to $v=3$ for the $A^2\Pi$ state of LaO have been determined. RKR potentials for the $A^2\Pi$ and $X^2\Sigma^+$ states were calculated and band strengths were obtained from the LEVEL program using an ab initio transition dipole function. Radiative lifetimes of the LaO $A^2\Pi$ state were also calculated. A line list is generated with PGOPHER for the $A^2\Pi$–$X^2\Sigma^+$ transition of LaO. This line list can be used to simulate LaO spectra in S-type stars.

Acknowledgments

The National Solar Observatory (NSO) is operated by the Association of Universities for Research in Astronomy, Inc. (AURA), under cooperative agreement with National Science Foundation. Financial support was provided by the NASA Laboratory Astrophysics Program (80NSSC21K1463). J.L. thanks the Consortium des Équipements de Calcul Intensif (CÉCI), funded by the Fonds de la Recherche Scientifique de Belgique (F.R.S.-FNRS) under grant No. 2.5020.11 and by the Walloon Region, for computational resources.

Software: PGOPHER (Western 2017), RKR (Le Roy 2017a), LEVEL (Le Roy 2017b), Excel (Microsoft), Wolfram Mathematica.

ORCID iDs

P. F. Bernath https://orcid.org/0000-0002-1255-396X
R. Dodangodage https://orcid.org/0000-0003-4814-4970

References

Bacis, R., Collomb, R., & Bessis, N. 1973, PhRvA, 8, 2255
Bernard, A., & Sibaï, A. 1980, ZNA, 35, 1313
Bernard, A., & Vergès, J. 2000, JMoSp, 201, 172
Bernath, P., Dodangodage, R., & Liévin, J. 2022, ApJ, 933, 99
Bernath, P. F. 2020, Spectra of Atoms and Molecules (Oxford: Oxford Univ. Press)
Brown, J., & Merer, A. 1979, JMoSp, 74, 488
Brown, J. M., & Carrington, A. 2003, Rotational Spectroscopy of Diatomic Molecules (Cambridge: Cambridge Univ. Press)
Cao, W., Zhang, Y., Wu, L., & Yang, D.-S. 2021, JPCA, 125, 1941
Carette, P., & Bencheikh, M. 1994, JMoSp, 163, 309
Childs, W., Goodman, G., Goodman, L., & Young, L. 1986, JMoSp, 119, 166
Hirota, E., Brown, J. M., Hougen, J., Shida, T., & Hirota, N. 1994, PApCh, 66, 571
Jevons, W. 1928, PPS, 41, 520
Johnson, J. A. 2019, Sci, 363, 474
Keenan, P. C. 1948, ApJ, 107, 420
Knowles, P. J., & Werner, H.-J. 1988, CPL, 145, 514
Le Roy, R. J. 2017a, JQSRT, 186, 158
Le Roy, R. J. 2017b, JQSRT, 186, 167
Lefebvre-Brion, H., & Field, R. W. 2004, The Spectra and Dynamics of Diatomic Molecules: Revised and Enlarged Edition (Amsterdam: Elsevier)
Liu, K., & Parson, J. 1977, JChPh, 67, 1814
MacConnell, D. J., Wing, R. F., & Costa, E. H. 2000, PASP, 112, 65
Nassau, J. 1956, VA, 2, 1361
Schoonveld, L., & Sundaram, S. 1974, ApJS, 27, 307
Steimle, T., & Virgo, W. 2002, JChPh, 116, 6012
Suenram, R., Lovas, F., Fraser, G., & Matsumura, K. 1990, JChPh, 92, 4724
Törring, T., Zimmermann, K., & Hoeft, J. 1988, CPL, 151, 520
Weltner, W., Jr., McLeod, D., Jr., & Kasai, P. H. 1967, JChPh, 46, 3172
Werner, H.-J., & Knowles, P. J. 1988, JChPh, 89, 5803
Werner, H.-J., Knowles, P. J., Knizia, G., Manby, F. R., & Schütz, M. 2012, Wiley Interdiscip. Rev. Comput. Mol. Sci., 2, 242
Werner, H.-J., Knowles, P. J., Knizia, G., et al. 2019, MOLPRO, v2019.2, a Package of ab initio Programs
Western, C. M. 2017, JQSRT, 186, 221
Ying, T., & Gang, J. 2020, Journal of Hebei University (Natural Science Edition), 40, 125